Polyhedron 76 (2014) 22–28

Contents lists available at ScienceDirect

Polyhedron

journal homepage: www.elsevier.com/locate/poly

Crystal structure, spectroscopic characterization and computational studies of a Re(I) tricarbonyl-diimine complex with the *N*,*N*′-bis(2-methylbenzaldehyde)-1,2-diiminoethane Schiff base

Akbar Rostami-Vartooni [a,*], Valiollah Mirkhani [b], Hadi Amiri Rudbari [b], Ahmad Jamali Moghadam [b]

[a] *Department of Chemistry, Faculty of Science, University of Qom, Qom 37185-359, Iran*
[b] *Faculty of Chemistry, University of Isfahan, Isfahan 81746-73441, Iran*

ARTICLE INFO

Article history:
Received 10 February 2014
Accepted 21 March 2014
Available online 2 April 2014

Keywords:
Tricarbonylrhenium(I) complexes
Diimine ligands
X-ray crystallography
TD-DFT
Electronic transition

ABSTRACT

The synthesis, structure and spectroscopic properties of a tricarbonylrhenium(I) complex with the *N*,*N*′-bis(2-methylbenzaldehyde)-1,2-diiminoethane Schiff base ligand have been investigated. This complex was characterized by FT-IR, NMR, UV–Vis spectroscopy and X-ray crystallography. Optimized geometric parameters and electronic properties of the synthesized compound and some similar Re(I) tricarbonyl complexes were obtained. The low lying electronic transition energies of the complexes have been determined with the time dependent density functional theory method. The calculations showed that in the complexes the HOMOs cover the Re atom, carbonyl groups and chlorine *p* orbitals, while the LUMOs are mainly localized on the diimine ligand as a π^* orbital.

1. Introduction

Rhenium complexes containing the *fac*-$[Re(CO)_3]^+$ moiety and derived from bifunctional Schiff base ligands show interesting photophysical and physicochemical properties [1,2], as well as being used as photosensitizers in solar cells [3,4], luminescence probes [5,6] and molecular parts of supramolecules [7]. The unique properties of Re(I) tricarbonyl-diimine complexes are closely connected to the existence of energetically low-lying charge transfer excited states with a large electron density shift from the metal to the diimine ligand (MLCT state) [8,9].

New advances in theoretical methods provide a convenient opportunity for the theoretical study of several important properties of organic and inorganic molecules. Recently, computational methods such as Density Functional Theory (DFT) and Time-Dependent Density Functional Theory (TD-DFT) have been used for the investigation of Molecular Orbitals (MOs), spectra and excited state structures of complexes [10–14]. Comprehensive studies on the ability of different DFT methods for rhenium complexes in geometry optimization and calculation of spectral properties have been reported in recent years [15,16].

In continuation of our recent works on amines and coordination chemistry [17,18], we have investigated the synthesis, structural and spectroscopic properties of $[Re(CO)_3(2\text{-m}'\text{bzen})Cl]$ (**1**), where 2-m′bzen is *N*,*N*′-bis(2-methylbenzaldehyde)-1,2-diiminoethane. Also, the optimized geometric parameters and electronic properties of the synthesized complex and similar compounds, $[Re(CO)_3(4\text{-nbzen})Cl]$ (**2**), $[Re(CO)_3(4\text{-bbzen})Cl]$ (**3**), $[Re(CO)_3(3\text{-bbzen})Cl]$ (**4**) and $[Re(CO)_3(3\text{-mbzen})Cl]$ (**5**) (see Scheme 1) that we have already investigated [19–21], were compared.

2. Experimental

2.1. General

$Re(CO)_5Cl$ (from Aldrich) and other starting materials were reagent grade and were used as received. The solvents were dried before use with the appropriate drying reagents. IR spectra were recorded on an IRPrestige-21 Shimadzu FT-IR instrument in KBr pellets. NMR spectra were obtained on a Brucker Avance 500 MHz spectrometer. Electronic spectra were recorded on a Shimadzu UV-160 spectrophotometer.

2.2. Synthesis of N,N′-bis(2-methylbenzaldehyde)-1,2-diiminoethane (2-m′bzen)

This ligand was prepared according to the literature [22,23]. Ethylendiamine (0.2 mL, 3 mmol) was added to a stirred solution of 2-methylbenzaldehyde (0.72 g, 6 mmol) in CH_2Cl_2 (15 mL). After

---

* Corresponding author. Tel.: +98 25 32103096; fax: +98 25 32850953.
E-mail address: a.rostami127@yahoo.com (A. Rostami-Vartooni).

http://dx.doi.org/10.1016/j.poly.2014.03.042
0277-5387/© 2014 Elsevier Ltd. All rights reserved.

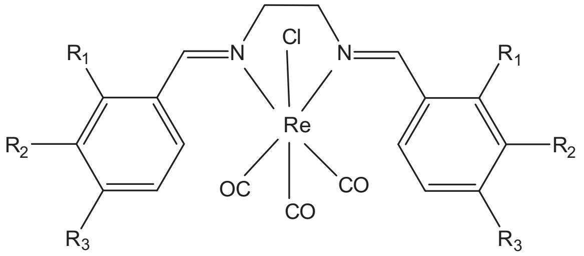

$R_1 = CH_3, R_2 = R_3 = H$ (**1**) $R_1 = R_2 = H, R_3 = NO_2$ (**2**)
$R_1 = R_2 = H, R_3 = Br$ (**3**) $R_1 = R_3 = H, R_2 = Br$ (**4**)
$R_1 = R_3 = H, R_2 = OCH_3$ (**5**)

Scheme 1.

Table 1
Crystal data and details of the structure determination of complex **1**.

Complex	**1**
Empirical formula	$C_{21}H_{22}ClN_2O_3Re$
Formula mass	572.02
Colour	colourless
Crystal system	monoclinic
Space group	$C2/c$
θ_{max}(°)	25.5
a (Å)	34.106(3)
b (Å)	10.9929(8)
c (Å)	19.5366(17)
α (°)	90
β (°)	119.567(6)
γ (°)	90
V (Å^3)	6370.9(10)
Z	12
D_{calc} (Mg/m^3)	1.789
μ (mm^{-1})	5.871
F(000)	3336
Index ranges	$-41 \leqslant h \leqslant 39$ $-13 \leqslant k \leqslant 13$ $-23 \leqslant l \leqslant 23$
No. of measured reflections	13335
No. of independent reflections/R_{int}	5088/0.086
No. of observed reflections $I > 2\sigma(I)$	4260
Number of parameters	383
Goodness-of-fit (GOF)	1.08
R_1 (observed data)	0.0632
wR_2 (all data)[a]	0.1620
Largest difference in peak and hole (e Å^{-3})	2.85 and −2.68

[a] $w = 1/[\sigma^2(F_o^2) + (0.0996P)^2 + 39.1940P]$, where $P = (F_o^2 + 2F_c^2)/3$.

stirring at room temperature for 3 h, the solution was filtered and the resulting solid was recrystallized from ethanol. Yield: 91%. FT-IR (KBr, cm^{-1}) ν_{max}: 1638 (C=N).

2.3. Synthesis of [Re(CO)$_3$(2-m′bzen)Cl]

A mixture of $Re(CO)_5Cl$ (0.2 g, 0.55 mmol) and 2-m′bzen (0.14 g, 0.55 mmol) in degassed CH_2Cl_2/toluene (30 mL, 1:2 V/V) was heated at reflux for 3 h. The solution was then concentrated to half volume and *n*-hexane was added to precipitate the crude material. The product was recrystallized from CH_2Cl_2/toluene to give pure crystals. Yield: 88%. *Anal.* Calc. for $C_{21}H_{22}ClN_2O_3Re$: C, 44.24; H, 3.71; N, 4.96. Found: C, 44.09; H, 3.88; N, 4.89%. FT-IR (KBr, cm^{-1}) ν_{max}: 2019, 1902, 1867 (CO); 1620 (C=N). ^{1}H NMR (d$_6$-DMSO, δ_{ppm}): 2.33 (s, 6H, 2 ($-CH_3$); 4.09–4.11, 4.34–4.38 (two sets of multiplets, 4H, $-CH_2-CH_2-$); 7.18–7.56 (m, 8H, aromatic hydrogens); 9.29 (s, 2H, iminic hydrogens).

2.4. Crystal structure determination

Single crystals, suitable for X-ray diffraction analysis, were grown by slow evaporation of a solution of the complex dissolved in CH_2Cl_2 and toluene (2:1). The crystallographic data and refinement parameters of the complexes are listed in Table 1. The X-ray single crystal data were collected at 296(1) K on a STOE IPDS 2T diffractometer (Mo Kα = 0.71073 Å). Cell parameters were retrieved using X-AREA [24] software and refined using X-AREA on all observed reflections. Data reduction and correction for Lp (Lorentz-polarization) and decay were performed using X-AREA software. Absorption corrections were applied using MULABS [25] in PLATON [26]. All structures were solved by direct methods and refined by full-matrix least squares on F^2 for all data using SHELXTL [27] software. All calculations were performed by PLATON.

2.5. Computational details

Ab initio calculations have been performed with the TURBOMOLE program package [28,29], making use of the resolution-of-the-identity (RI) approximation for the evaluation of the electron-repulsion integrals. The equilibrium geometries at the ground electronic states (S_0) have been determined at the Möller–Plesset second order perturbation theory (MP2) level. The calculations were performed with a few basis sets, the effective core potential (ECP, based on the TURBOMOLE 6.2 program default) was used for rhenium (Re) and the correlation-consistent polarized valence double-zeta (cc-pVDZ) [30] basis sets were used for all the other atoms, i.e. except Re. The charge distribution calculations were performed based on the Natural Population Analysis algorithm (NPA) implemented in the TURBOMOLE program package [31]. TD-DFT using the B3LYP (Becke, three-parameter, Lee–Yang–Parr) functional was applied to compute the vertical electronic transition energies and the oscillator strengths of the complexes. The geometries from the X-ray structural data of the selected complexes were used as the initial geometries in the optimization calculations.

3. Results and discussions

3.1. General characterization

The obtained complex is stable in air, either as a solid or in solution, and was characterized by the usual spectroscopic techniques. Coordination of the ligand is indicated by the shifts of ν(C=N) from 1638 cm^{-1} in the free ligand to 1620 cm^{-1} in the related complex. The IR spectrum of the complex shows three lower energy and sharp intense bands in the carbonyl range 1865–2023 cm^{-1} [32,33]. The ^{1}H NMR spectrum of the complex shows the $-CH_2-CH_2-$ groups as two sets of multiplets, indicating that these protons are not equivalent. The electronic absorption spectroscopic data of the 2-m′bzen ligand and the related Re complex in CH_2Cl_2 are included in Table 2. In tricarbonylrhenium(I) complexes, the bands observed at 230–300 nm may be due to $\pi \rightarrow \pi^*$ transitions and the long wavelength absorption bands (above 350 nm) are assigned to MLCT transitions from Re(I) to π^* (ligand) [34,35].

Table 2
Electronic absorption spectral data of the 2-m′bzen ligand and complex **1** in CH_2Cl_2.

Compound	Concentration (M)	λ_{max}/nm (ε/M^{-1}cm^{-1})
2-m′bzen	8×10^{-5}	250 [21850]
[Re(CO)$_3$(2-m′bzen)Cl]	4×10^{-5}	231 [16600], 261 [18350], 359 [1632][a]

[a] 1×10^{-3} M.

3.2. Molecular structure

A perspective drawing and the crystal packing of complex **1** are shown in Figs. 1 and 2. The metal center has an almost ideal octahedral coordination sphere with a facial arrangement of three carbonyl groups. The axially disposed chloro and carbonyl ligands are also disordered over two positions around the crystallographic twofold rotation axis, with a half site occupancy factor in each position. As shown in Table 3, no significant influence of the different substituents is seen on the bonds and angles in this complex and in similar compounds investigated previously [19–21]. The values of the diimine bite angles [77.4(3)° and 77.9(5)°] slightly

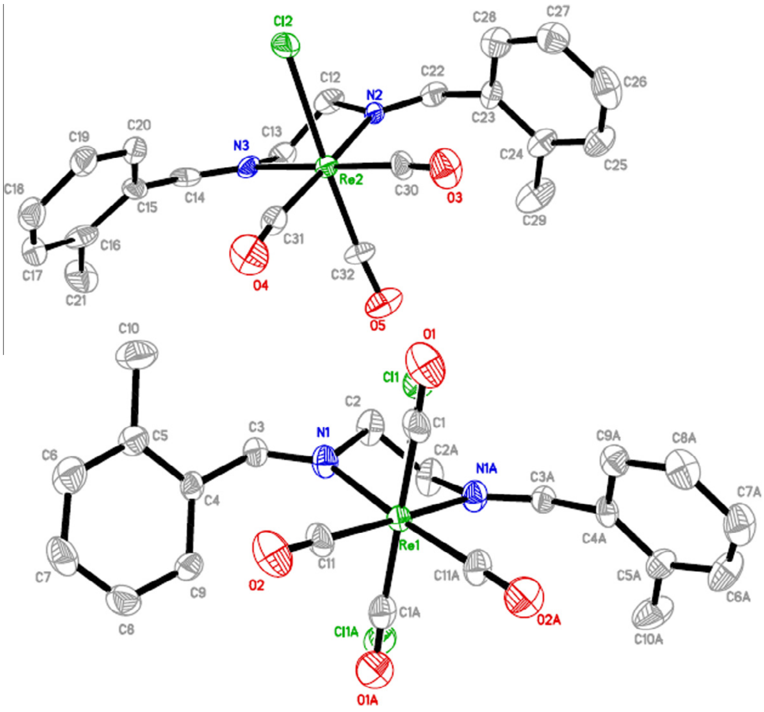

Fig. 1. The molecular structure of complex **1**, showing 50% probability displacement ellipsoids and the atomic numbering.

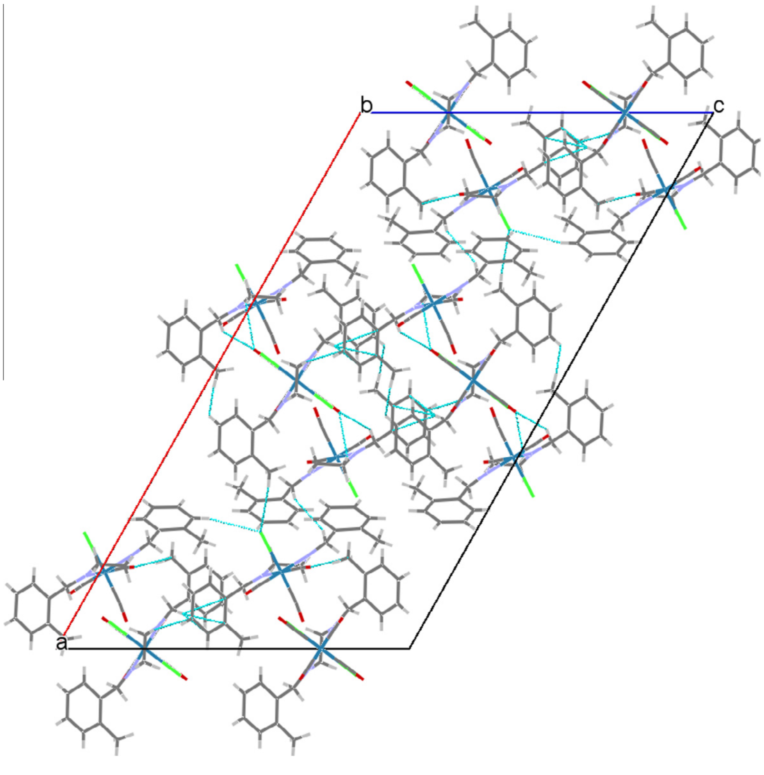

Fig. 2. The crystal packing of complex **1**, showing the linkage of molecules by intermolecular interactions.

deviate from the expected ideal 90° for an octahedron. Hydrogen bonding interactions for the synthesized complex are summarized in Table 4. An interesting feature of the crystal packing is the intermolecular C–H···O interactions in which the oxygen atom is a bifurcated acceptor (Fig. 2).

3.3. Geometries, electronic structures and electronic spectra

The optimized geometry of complex **1** and several of the highest occupied (HOMO−5 to HOMO) and the lowest unoccupied (LUMO to LUMO+5) orbitals of complex **5** are presented in Figs. 3 and 4. A comparison of the energy level and configuration of the HOMOs and LUMOs of complexes **1**–**5** are shown in Fig. 5. Also, more information about the geometries and energetic diagrams of the frontier orbitals of complexes **1**–**5** are presented in the electronic Supplementary information file (ESI) (see Figs. SM1–SM9). As shown in these figures, the highest three occupied molecular orbitals in the complexes are predominately located on the Re atom, which correspond to the $(5d_{xy})^2(5d_{yz})^2(5d_{xz})^2$ occupation of the central ion.

The HOMO and HOMO−1 orbitals of complexes **1**, **2** and **3** are of the d type with some contribution from p_π chloride and the π-antibonding orbital of the CO ligands. In complex **5**, the HOMO is located on the benzene ring, while the d_{Re} orbitals take a main part in the HOMO−1 to HOMO−4 orbitals. The low-lying virtual orbitals mainly correspond to $\pi^*_{diimine}$ orbitals ($\pi^*_{C=C}$, $\pi^*_{C=N}$ or $\pi^*_{N=O}$ in the case of the nitro substituted complex). The energy of $\pi^*_{diimine}$ is lower than that of the π^*_{CO} orbitals and the HOMO–LUMO energy gap is 10.39, 9.36, 10.0, 10.05 and 10.10 eV for complexes **1**–**5**, respectively.

The experimental and optimized geometric parameters of complexes **2**–**5** are presented in Table 5. As shown in Tables 3 and 5, the MP2 calculated values using the cc-pVDZ basis set for selected bond lengths and bond angles in the Re complexes are well comparable with the X-ray experimental data. Therefore the MP2/cc-pVDZ level of calculation is convenient to obtain geometric parameters for such inorganic compounds. Due to the π-donor character of the chloride ligand, the Re–C(3) (see Fig. 3) bond length in the complexes is slightly shorter than the Re–C(1) and Re–C(2) bond lengths, which are relatively consistent with the

Table 3
Selected experimental and optimized bond lengths (Å) and bond angles (°) of complex **1**. The theoretical values are in brackets.

Bond lengths		Bond angles	
Re(1)–Cl(1)	2.500(10)	N(1)–Re(1)–N(1A)	77.9(5)
Re(2)–Cl(2)	2.490(3) [2.497]	N(2)–Re(2)–N(3)	77.4(3) [75.9]
Re(1)–N(1)	2.214(10)	N(1)–Re(1)–C(11)	97.5(5)
Re(2)–N(2)	2.189(8) [2.216]	N(2)–Re(2)–C(30)	100.7(4) [98.3]
Re(2)–N(3)	2.196(9) [2.216]	N(3)–Re(2)–C(31)	97.2(5) [101.9]
Re(1)–C(1)	1.79(3)	C(1)–Re(1)–Cl(1A)	177.0(9)
Re(1)–C(11)	1.949(12)	C(1)–Re(1)–C(1A)	175.4(19)
Re(2)–C(32)	1.902(13) [1.890]	C(32)–Re(2)–Cl(2)	175.3(4) [173.0]
Re(2)–C(31)	1.946(11) [1.918]	Cl(1)–Re(1)–N(1)	82.4(3)
Re(2)–C(30)	1.932(12) [1.917]	Cl(1)–Re(1)–N(1A)	89.9(3)
N(1)–C(3)	1.273(15)	Cl(2)–Re(2)–N(2)	81.6(2) [87.0]
N(2)–C(22)	1.266(14) [1.300]	Cl(2)–Re(2)–N(3)	86.5(3) [79.6]
N(3)–C(14)	1.284(15) [1.296]		

Table 4
Parameters of the hydrogen bonding interactions in complex **1**.

D–H···A	H···A (Å)	D···A (Å)	D–H···A (°)
C(12)–H(12A)···O(1)^i	2.65	3.33(3)	127.1
C(22)–H(22B)···O(1)^i	2.63	3.50(3)	149.4

Symmetrycode: (i) $x, -1 + y, z$.

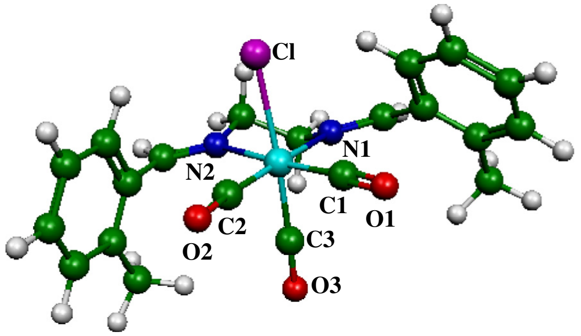

Fig. 3. Optimized geometry structure of complex **1**, at the MP2/cc-pVDZ level of theory.

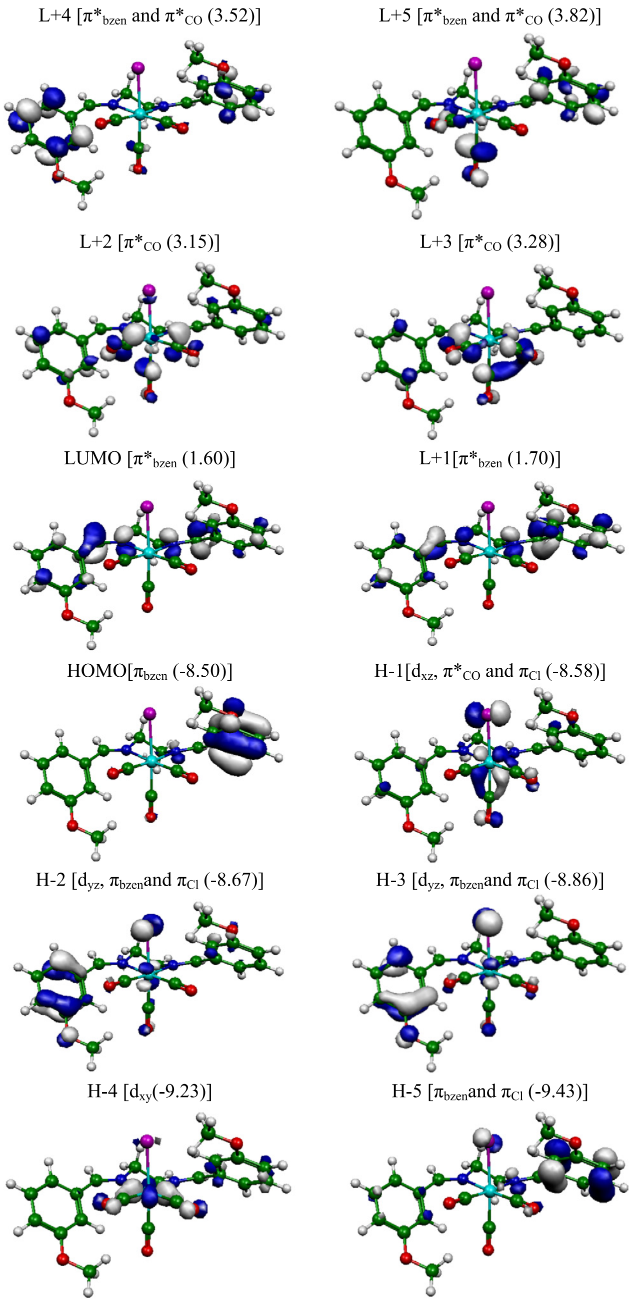

Fig. 4. The highest six occupied (HOMO−5 to HOMO) and the lowest six unoccupied (LUMO to LUMO+5) orbitals of complex **5**. The configuration and energy level (in eV) of the orbitals are in brackets.

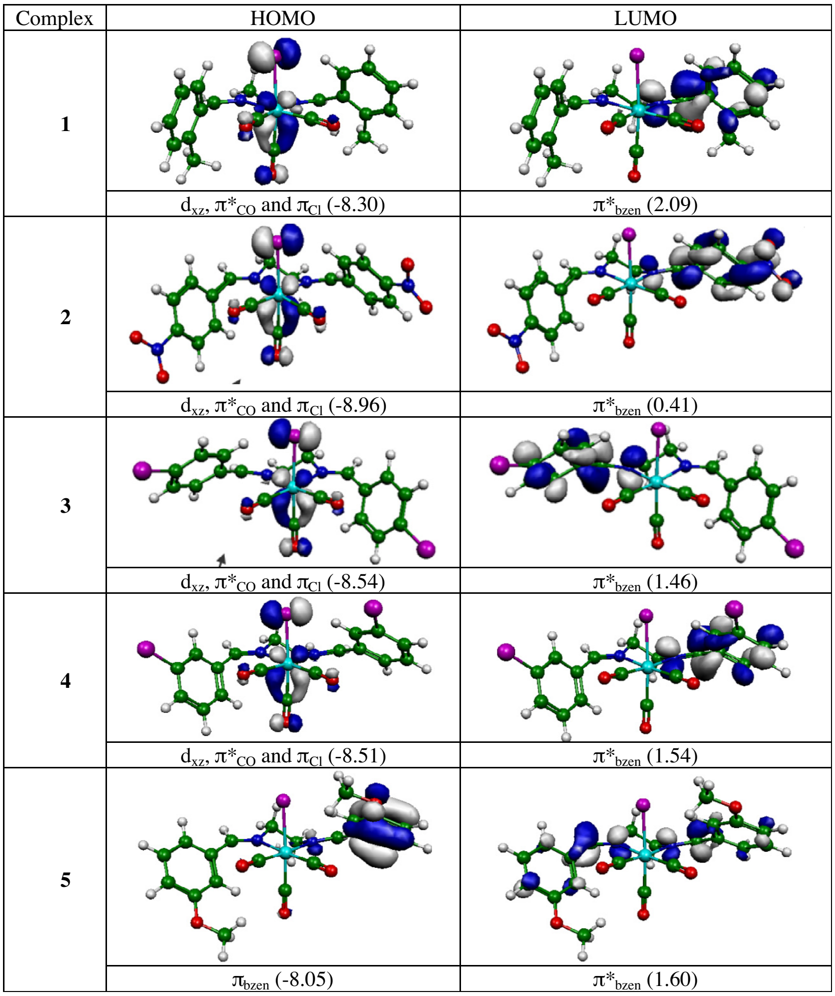

Fig. 5. A comparison of the energy levels (in eV) and configurations of the HOMOs and LUMOs of complexes **1**–**5**.

Table 5
Selected experimental and optimized bond lengths (Å) and bond angles (°) of complexes **2**–**5**. The theoretical values are in brackets and X-ray data taken from the literatures are presented out of the brackets.

Complex	**2**[a]	**3**[b]	**4**[c]	**5**[b]
Bond lengths				
Re–Cl	2.4814(9) [2.515]	2.4929(7) [2.517]	2.4884(11) [2.515]	2.4835(10) [2.517]
Re–N(1)	2.212(2) [2.220]	2.225(2) [2.223]	2.206(4) [2.222]	2.195(3) [2.225]
Re–N(2)	2.217(3) [2.221]	2. 188(3) [2.223]	2.208(3) [2.223]	2.199(3) [2.237]
Re–C(1)	1.916(4) [1.915]	1.913(3) [1.917]	1.897(4) [1.915]	1.929(4) [1.911]
Re–C(2)	1.921(4) [1.916]	1.937(3) [1.914]	1.909(5) [1.917]	1.912(4) [1.915]
Re–C(3)	1.911(5) [1.893]	1.918(3) [1.891]	1.899(5) [1.891]	1.913(4) [1.889]
Bond angles				
N(1)–Re–N(2)	77.01(10) [76.2]	78.15(8) [76.3]	77.28(13) [76.2]	77.73(11) [76.7]
N(1)–Re–C(1)	98.16(13) [100.0]	98.14(11) [98.7]	101.14(17) [100.4]	97.17(15) [99.6]
N(2)–Re–C(2)	98.93(14) [99.1]	98.62(10) [100.3]	97.66(16) [98.7]	99.48(15) [99.5]
C(1)–Re–C(3)	89.78 (16) [86.8]	86.86(12) [89.0]	88.43(19) [86.6]	90.87(18) [86.0]
C(2)–Re–C(3)	88.37(16) [89.0]	92.08(11) [86.7]	91.5(2) [89.0]	86.58(18) [89.3]
C(3)–Re–Cl	176.90(12) [174.4]	173.53(9) [174.8]	175.40(16) [174.7]	175.83(13) [175.1]

[a] The experimental values were taken from Reference 19.
[b] The experimental values were taken from Reference 20.
[c] The experimental values were taken from Reference 21.

experimental results. The reason can be related to the presence of extended π-bonding between the π orbital of ligand in the trans position to the Re–C(3) bond and the Re d$_\pi$ orbital, which weakens the Re → C(3) back bonding [16].

Table 6 shows a summary of the charge distribution calculations for each complex. The charge values on the rhenium atom in the complexes are significantly lower than the formal charge of +1, which corresponds to a d^6 configuration of the central ion.

Table 6
Selected atomic charge distribution, calculated based on the Natural Population Analysis algorithm (NPA). The complex numbering is performed based on Fig. 3.

Complex	**1**	**2**	**3**	**4**	**5**
Re	−0.132	−0.15	−0.144	−0.145	−0.125
N(1)	−0.6	−0.587	−0.585	−0.596	−0.613
N(2)	−0.582	−0.575	−0.601	−0.582	−0.603
Cl	−0.661	−0.649	−0.653	−0.649	−0.649
C(1)	0.771	0.767	0.786	0.767	0.763
C(2)	0.776	0.786	0.767	0.787	0.784
C(3)	0.713	0.71	0.71	0.71	0.708
O(1)	−0.596	−0.592	−0.589	−0.594	−0.599
O(2)	−0.596	−0.589	−0.595	−0.589	−0.592
O(3)	−0.636	−0.626	−0.632	−0.634	−0.637

A significant charge donation from the ligands to the Re atom is the reason for such a low charge being located on the central Re atom [36]. The oxygen atom which is exactly in front of the chloride ion has the highest negative charge, as a result of the π-donor character of the chloride ligand.

Typically, the vertical electronic transition energies accompanied with their oscillator strengths for complexes **1**–**5** have been obtained at the TD-DFT/cc-PVDZ level of theory on the optimized geometries (see Table 7). The discrepancy between the experimental and theoretical results in Table 7 originates from two sources. The theoretical results are vertical transitions, not adiabatic, and obviously they will be far from either the adiabatic or the experimental transitions. Another source will be related to solvent effects, which were not considered in the calculations. The broad low-energy absorption band at about 370–390 nm is attributed to Metal–Ligand Charge Transfer transitions (MLCT), occurring from the rhenium center to the π* diimine orbitals (d → π*). The mixed $d_{Re} + \pi^*_{CO}/\pi_{Cl}$ character of the HOMO and HOMO−1 orbitals implies that the transitions can be seen as mixed Re → bzen (MLCT) and Cl → bzen (LLCT), or a delocalized MLLCT (metal-ligand-to-ligand CT) description can be used. The lowest-lying absorptions, which arise from the HOMO → LUMO excitation configuration, are red-shifted in the order **2** < **4** < **3** < **5** < **1**, when the electron-withdrawing substituents are introduced into the benzene ring. The energy levels of the LUMO for complexes **1**–**5** are 2.09, 0.41, 1.46, 1.54 and 1.60 eV, respectively. Obviously, the LUMO is more stabilized with the electron-withdrawing substituent in the complex **2**. This is quite in agreement with previously reported results on the stabilization of π* orbitals of aromatic molecules by an electron-withdrawing group [37,38].

Table 7
The lowest lying transition energies and oscillator strengths of complexes **1**–**5**, calculated at the TD-DFT/cc-pVDZ level of theory.

λ (nm)	E(eV)	Oscillator Strength	The most important orbital excitations	Character	Experimental λ (nm)[a]
1					
404.3	3.07	0.0294	H → L (91.4%)	$d_{xz} + \pi^*_{CO}/\pi_{Cl} \rightarrow \pi^*$(bzen)	391[b]
387.5	3.2	0.0091	H−1 → L (82.2%)	$d_{yz} + \pi_{Cl} \rightarrow \pi^*$(bzen)	261
375	3.31	0.0102	H → L+1 (82.4%)	$d_{xz} + \pi^*_{CO}/\pi_{Cl} \rightarrow \pi^*$(bzen)	
359	3.45	0.026	H−1 → L+1 (94.2)	$d_{yz} + \pi_{Cl} \rightarrow \pi^*$(bzen)	
354.5	3.5	0.0028	H−2 → L+1 (93.9)	$d_{xy} \rightarrow \pi^*$(bzen)	
2					
489.6	2.53	0.0181	H → L (90.8%)	$d_{xz} + \pi^*_{CO}/\pi_{Cl} \rightarrow \pi^*$(bzen)	391[b]
468.1	2.65	0.0187	H−1 → L (62.1%)	$d_{yz} + \pi_{Cl} \rightarrow \pi^*$(bzen)	261
			H → L+1 (32.6%)	$d_{xz} + \pi^*_{CO}/\pi_{Cl} \rightarrow \pi^*$(bzen)	
464	2.67	0.0028	H → L+1 (60.2%)	$d_{xz} + \pi^*_{CO}/\pi_{Cl} \rightarrow \pi^*$(bzen)	
			H−1 → L (30.0%)	$d_{yz} + \pi_{Cl} \rightarrow \pi^*$(bzen)	
443.2	2.8	0.016	H−1 → L+1 (94.1%)	$d_{yz} + \pi_{Cl} \rightarrow \pi^*$(bzen)	
404	3.07	0.0014	H−2 → L (95.6%)	$d_{xy} \rightarrow \pi^*$(bzen)	
3					
429.5	2.89	0.0298	H → L (93.5%)	$d_{xz} + \pi^*_{CO}/\pi_{Cl} \rightarrow \pi^*$(bzen)	370[b]
412.6	3.01	0.0066	H−1 → L (58.0%)	$d_{yz} + \pi_{Cl} \rightarrow \pi^*$(bzen)	261
			H → L+1 (40.3%)	$d_{xz} + \pi^*_{CO}/\pi_{Cl} \rightarrow \pi^*$(bzen)	233
404.3	3.07	0.0116	H → L+1 (54.1%)	$d_{xz} + \pi^*_{CO}/\pi_{Cl} \rightarrow \pi^*$(bzen)	
			H−1 → L (37.7%)	$d_{yz} + \pi_{Cl} \rightarrow \pi^*$(bzen)	
390.1	3.18	0.0371	H−1 → L+1 (96.5%)	$d_{yz} + \pi_{Cl} \rightarrow \pi^*$(bzen)	
365.5	3.39	0.0002	H−2 → L (95.0%)	$d_{xy} \rightarrow \pi^*$(bzen)	
4					
432.5	2.87	0.0202	H → L (94.8%)	$d_{xz} + \pi^*_{CO}/\pi_{Cl} \rightarrow \pi^*$(bzen)	374[b]
415.3	2.99	0.0063	H−1 → L (57.2%)	$d_{yz} + \pi_{Cl} \rightarrow \pi^*$(bzen)	254
			H → L+1 (40.9%)	$d_{xz} + \pi^*_{CO}/\pi_{Cl} \rightarrow \pi^*$(bzen)	
406.5	3.05	0.0106	H → L+1(53.3%)	$d_{xz} + \pi^*_{CO}/\pi_{Cl} \rightarrow \pi^*$(bzen)	
			H−1 → L (39%)	$d_{yz} + \pi_{Cl} \rightarrow \pi^*$(bzen)	
392.9	3.16	0.0319	H−1 → L+1 (95.6%)	$d_{yz} + \pi_{Cl} \rightarrow \pi^*$(bzen)	
367.8	3.37	0.0004	H−2 → L (95.6%)	$d_{xy} + \pi$ (bzen)/$\pi_{Br} \rightarrow \pi^*$(bzen)	
5					
411.3	3.01	0.0164	H → L (98.6%)	π(bzen) → π*(bzen)	369[b]
395.6	3.13	0.005	H → L+1 (51.1%)	π(bzen) → π*(bzen)	258
			H−1 → L (47.4%)	$d_{xz} + \pi^*_{CO}/\pi_{Cl} \rightarrow \pi^*$(bzen)	238
387.6	3.2	0.0065	H−1 → L (49.6%)	$d_{xz} + \pi^*_{CO}/\ \pi_{Cl} \rightarrow \pi^*$(bzen)	
			H → L+1 (47.6%)	π(bzen) → π*(bzen)	
377.3	3.29	0.0452	H−1 → L+1(96.3%)	$d_{xz} + \pi^*_{CO}/\pi_{Cl} \rightarrow \pi^*$(bzen)	
357	3.47	0.0635	H−2 → L (53.3%)	$d_{yz} + \pi$(bzen)/$\pi_{Cl} \rightarrow \pi^*$(bzen)	
			H−4 → L (24.2%)	$d_{xy} \rightarrow \pi^*$(bzen)	

H represents the highest occupied orbital (HOMO) and L represents to the lowest unoccupied orbital (LUMO).

[a] Solvent = dichlorometane.

[b] $C = 1 \times 10^{-3}$ M.

4. Conclusion

In this work, we report the synthesis, structural, spectroscopic and computational studies of a Re(I) tricarbonyl-diimine complex with the *N*,*N*′-bis(2-methylbenzaldehyde)-1,2-diiminoethane Schiff base ligand. The ground state optimized geometry parameters of the synthesized compound and four similar complexes at the MP2/cc-pVDZ level of theory are in good agreement with the X-ray experimental data. The molecular orbital diagrams of the complexes, with the several highest occupied and lowest unoccupied molecular orbital contours, showed that the highest occupied MOs are of the d type with some contributions from p_π chloride and π^* orbitals localized on the CO part of the compex. The lowest vacant orbitals correspond to π^* orbitals localized on the diimine ligand. The UV–Vis spectra of compounds could be discussed on the bases of the TD-DFT calculations. The calculated charge distributions showed values between −0.125 and −0.15 q on the Re atom, which is in accordance with the charge donation character of the ligands.

Acknowledgements

This work was supported by the University of Qom and the University of Isfahan. The authors are grateful for their support. AR thanks Dr. Reza Kia for the structure solution and refinement of the complex.

Appendix A. Supplementary data

CCDC 978385 contains the supplementary crystallographic data for complex **1**. These data can be obtained free of charge via http://www.ccdc.cam.ac.uk/conts/retrieving.html, or from the Cambridge Crystallographic Data Centre, 12 Union Road, Cambridge CB2 1EZ, UK; fax: +44 1223 336 033; or e-mail: deposit@ccdc.cam.ac.uk. Supplementary data associated with this article can be found, in the online version, at http://dx.doi.org/10.1016/j.poly.2014.03.042.

References

[1] M. Vlček Jr., Coord. Chem. Rev. 250 (2006) 1755.
[2] D.R. Striplin, G.A. Crosby, Coord. Chem. Rev. 211 (2001) 163.
[3] M. Grätzel, Energy Resources through Photochemistry and Catalysis, Academic Press, New York, 1983.
[4] Y. Chen, W. Liu, J.S. Jin, B. Liu, Z.G. Zou, J.L. Zuo, X.Z. You, J. Organomet. Chem. 694 (2009) 763.
[5] A. Vogler, H. Kunkely, Coord. Chem. Rev. 200 (2000) 991.
[6] S.S. Jurisson, J.D. Lydon, Chem. Rev. 99 (1999) 2205.
[7] S. Uhlenbrock, R. Wegner, B. Krebs, J. Chem. Soc., Dalton Trans. 36 (1996) 3731.
[8] N. Iznaga-Escobar, Nucl. Med. Biol. 25 (1998) 441.
[9] E.A.D. Eutsch, K. Libson, J.L. Vanderheyden, Technetium and Rhenium in Chemistry and Nuclear Medicine, Raven Press, New York, 1990.
[10] J. Su, L. Shi, X. Sun, W. Guan, Z. Wu, Dalton Trans. 40 (2011) 11131.
[11] S. Salehzadeh, R. Golbedaghi, I.S. Tidmarsh, N.K. Al-Rasbi, H. Adams, M.D. Ward, Polyhedron 27 (2008) 3549.
[12] C. Makedonas, C.A. Mitsopoulou, Inorg. Chim. Acta 360 (2007) 3997.
[13] N. Matsuoka, N. Yoshioka, Chem. Phys. Lett. 523 (2012) 65.
[14] J.F. Yin, D. Bhattacharya, P. Thanasekaran, C.P. Hsu, T.W. Tseng, K.L. Lu, Inorg. Chim. Acta 362 (2009) 5064.
[15] J. Gancheff, P.A. Denis, F.E. Hahn, J. Mol. Struct. (Theochem) 941 (2010) 1.
[16] B. Machura, J. Kusz, D. Tabak, R. Kruszynski, Polyhedron 28 (2009) 493.
[17] M. Nasrollahzadeh, A. Ehsani, A. Rostami-Vartouni, Ultrason. Sonochem. 21 (2014) 275.
[18] M. Nasrollahzadeh, A. Rostami-Vartooni, A. Ehsani, M. Moghadam, J. Mol. Catal. A: Chem. 387 (2014) 123.
[19] V. Mirkhani, R. Kia, A.R. Vartooni, D. Milic, Transition Met. Chem. 34 (2009) 225.
[20] V. Mirkhani, R. Kia, A.R. Vartooni, H.K. Fun, Polyhedron 29 (2010) 1600.
[21] V. Mirkhani, R. Kia, D. Milic, A.R. Vartooni, D. Matkovic-Calogovic, Transition Met. Chem. 35 (2010) 81.
[22] A. Ghaffarinia, H. Golchoubian, R. Hosseinzadeh, J. Chin. Chem. Soc. 52 (2005) 531.
[23] R. Hosseinzadeh, H. Golchoubian, M. Masoudi, J. Chin. Chem. Soc. 55 (2008) 649.
[24] Stoe & Cie, X-AREA, Stoe & Cie, Darmstadt, Germany, 2005.
[25] R.H. Blessing, Acta Crystallogr., Sect. A 51 (1995) 33.
[26] A.L. Spek, Acta Crystallogr., Sect. D 65 (2009) 148.
[27] G.M. Sheldrick, Acta Crystallogr., Sect. A 64 (2008) 112.
[28] R. Ahlrichs, M. Bar, M. Haser, H. Horn, C. Kolmel, Chem. Phys. Lett. 162 (1989) 165.
[29] Turbomole V6.3, A Development of the University of Karlsruhe and Forschungazentrum Karlsruhe GmbH, 1989–2007, Turbomole, GmbH, since 2007. Available from: <http://www.turbomole.com>.
[30] T.H. Dunning, J. Chem. Phys. 90 (1989) 1007.
[31] A.E. Reed, R.B. Weinstock, F. Weinhold, J. Chem. Phys. 93 (1985) 735.
[32] E. Wolcan, G. Torchia, J. Tocho, O.E. Piro, P. Juliarena, G. Ruiz, M.R. Feliz, J. Chem. Soc., Dalton Trans. (2002) 2194.
[33] A. Klein, C. Vogler, W. Kaim, Organometallics 15 (1996) 236.
[34] M.K. Itokazu, A.S. Polo, N.Y. Murakami Iha, J. Photochem. Photobiol., A 160 (2003) 27.
[35] M. Busby, P. Matousek, M. Towrie, A. Vlček Jr., Inorg. Chim. Acta 360 (2007) 885.
[36] B. Machura, M. Wolff, L. Gryca, A. Palion, K. Michalik, Polyhedron 30 (2011) 2275.
[37] V.M. Miskowski, V.H. Houlding, C.M. Che, Y. Wang, Inorg. Chem. 32 (1993) 2518.
[38] C.S.K. Mak, H.L. Wonga, Q.Y. Leung, W.Y. Tama, W.K. Chan, A.B. Djurisic, J. Organomet. Chem. 694 (2009) 2770.